Lattice strain measurements of deuteride (hydride) formation in epitaxial Nb: Additional results and further insights into past measurements

Monica M. C. Allain* and Brent J. Heuser†
University of Illinois, Department of Nuclear, Plasma, and Radiological Engineering, Urbana, Illinois 61801, USA
(Received 21 March 2005; revised manuscript received 14 June 2005; published 1 August 2005)

The evolution of lattice strain during *in situ* gas-phase deuterium loading of epitaxial $(1\bar{1}0)$ Nb films on the $(11\bar{2}0)$ sapphire was measured with x-ray diffraction. Two samples with film thicknesses 208 and 1102 Å were driven through the miscibility gap. Strains in three orthogonal directions were recorded, permitting the complete set of unit cell parameters to be determined for both the solid solution and deuteride phases. The overall film thickness was simultaneously measured by recording the glancing angle reflectivity response. The behavior of the two films was markedly different, with the thicker film exhibiting a much more compliant behavior and concomitant irreversible plastic deformation. The correlation between out-of-plane lattice and film expansion for both films is also consistent with this observation. These results help explain past inconsistencies observed by others.

DOI: 10.1103/PhysRevB.72.054102 PACS number(s): 64.70.Nd, 61.10.Nz, 61.72.Hh, 68.55.Nq

I. INTRODUCTION

The study of hydrogen in Nb-based restricted-geometry systems dates to the 1980s, when Miceli and Zabel examined elastically mediated critical fluctuations in Nb-Ta superlattice structures in a series of *in situ* x-ray diffraction (XRD) experiments.[1,2] This work demonstrated that critical fluctuations arising from the long-range elastic hydrogen-hydrogen interaction are suppressed at low hydrogen concentrations for wavelengths shorter than the superlattice period. As a consequence, phase separation into gaslike and liquidlike phases associated with the lattice gas model cannot take place. One-dimensional lattice expansion normal to the plane of the film was found to be characteristic of the suppressed phase separation.[2,3] This anisotropic expansion becomes unstable at high hydrogen concentration, and hydride formation eventually occurs.[3]

Hydrogen in single-layer Nb films has been extensively studied over the last ten years. This work has mostly used epitaxial $(1\bar{1}0)$ Nb films, since this orientation grows nearly strain-free on $(11\bar{2}0)$ sapphire during MBE deposition conditions.[4] This newer body of work has focused on the perturbation of the Nb-hydrogen phase diagram in thin film geometry and arguably originates with Alefeld.[5] Alefeld demonstrated that the hydrogen-hydrogen interaction, which is elastic in nature, is weakened, even made repulsive, when the host lattice is constrained by boundary conditions that inhibit volume expansion. The adhesion of a hydrogen-absorbing thin film to a nonabsorbing substrate imposes a clamping stress that, at least in the plane of the film, inhibits expansion. The result of this inhibited expansion and associated reduction of the hydrogen-hydrogen interaction energy is a lower critical point temperature. The miscibility gap is thereby suppressed and continuous phase behavior is observed below the bulk Nb-H critical point. A second important consequence of the in-plane clamping stress is enhanced out-of-plane strain beyond the isotropic expansion expected from bulk Nb. Ideally, this strain anisotropy should follow the one-dimensional expansion of a clamped elastic medium.[6]

The effect of restricted geometry on the phase behavior of hydrogen in epitaxial Nb has been investigated by Song *et al.* in a series of pressure versus out-of-plane lattice strain isothermal XRD measurements.[7] The isothermal dependence on film thickness was determined above the critical point over a large concentration range. Fits using a standard thermodynamic model yielded the hydrogen-hydrogen interaction energy and the critical temperature as a function of film thickness. This work demonstrates that both the hydrogen-hydrogen interaction energy and critical point decrease systematically with decreasing epitaxial film thickness. Strain anisotropy in the same system was investigated by Song *et al.* with XRD, and the results were used to estimate the in-plane clamping stress (~3.5 GPa).[8]

Sievert's region (low hydrogen concentration) in epitaxial $(1\bar{1}0)$ Nb has been investigated by Johansson *et al.* as a function of film thickness and temperature.[9] Four-point probe resistivity measurements were used to estimate the overall hydrogen concentration in the films. As expected, the solubility of hydrogen is reduced considerably compared to bulk and increases with film thickness up to a thickness of 500 Å. Slight deviations from the continuous linear behavior associated with Sievert's law were observed and attributed to a different hydrogen absorption potential in the film near the substrate.[9]

The validity of Vegard's law (the linear behavior of lattice strain versus concentration) in single-layer epitaxial Nb has been investigated at low hydrogen concentration by Reimer *et al.*[6] and at high concentration by Abromeit *et al.*[10] Enhanced out-of-plane expansion was observed at low concentration ($\leqslant 0.02$ [H]/[Nb]) at room temperature that exceeds by a factor of 4 the anisotropic one-dimensional expansion expected from a clamped elastic medium.[6] The expected one-dimensional expansion was observed at high concentration (~1[H]/[Nb]) above the critical point in a 320 Å thick film by Abromeit *et al.*[10] The out-of-plane strain of a thicker film (780 Å), again above the critical point, exhibited the behavior expected from bulk Nb,[10] somewhat at variance, with the generally accepted behavior of thin film Nb. It is

important to note that the observation of out-of-plane bulklike expansion in thin-film Nb does not necessarily imply equivalent in-plane expansion. In fact, conclusive evidence exists to the contrary.[3,8] Laudahn *et al.* examined the elastic response of 1900 Å single-layer epitaxial and textured $(1\bar{1}0)$ Nb films and observed a one-dimensional expansion behavior at low concentration ($\leqslant 0.2$[H]/[Nb]).[11]

Related investigations of anisotropic expansion have been performed with Nb-based multilayers by Yang *et al.*[12] and by Rehm *et al.*[13] The former tracked the out-of-plane lattice expansion of the Nb component of Nb/Pd multilayers as a function of hydrogen concentration. The expected one-dimensional expansion was observed at room temperature for hydrogen concentrations within the solid solution α phase, but only after prior cycling across the miscibility gap. A cycling-induced reversal of the strain state (out of plane: tensile $\rightarrow$ compressive; in plane: compressive $\rightarrow$ tensile) was also observed by Yang *et al.* This reversal was thought to be coupled to plastic instability associated with the $\alpha \rightarrow \alpha'$ phase transformation.[12] The origin of this irreversible strain was not conclusively identified, however. Rehm *et al.* were the first to track both the Nb layer thickness change and out-of-plane Nb lattice strain *in situ* as a function of the hydrogen concentration. These authors used Nb-Fe multilayers and found that the former exceeded the latter by a factor of 2 at saturation above the critical point. This observation was attributed to the creation of additional volume during hydrogen absorption. Rehm *et al.* suspected voids at grain boundaries were the source of the extra volume.[13]

It is interesting to note that both Yang *et al.* and Rehm *et al.* observed out-of-plane lattice expansion equal to that of bulk Nb (as opposed to the anisotropic one-dimensional expansion of a clamped elastic medium) during the *first* hydrogen absorption cycle. The only common feature of these two investigations was that the Nb was part of a textured or polycrystalline multilayer structure. The temperature (Ref. 12: $T<T_c$; Ref. 13: $T>T_c$), Nb layer thickness (Ref. 12: ~140 Å; Ref. 13: 1000 Å), and hydrogen concentration (Ref. 12: $0.02<$[H]/[Nb]<0.17; Ref. 13: $0.1<$[H]/[Nb]<1) were all significantly different. As mentioned above, Abromeit *et al.* also observed out-of-plane strain equal to that of bulk Nb, evidently during the first hydrogen absorption cycle as well.

One possible explanation is that bulklike out-of-plane expansion is a characteristic of virgin thin-film Nb. However, Rehm *et al.* did not believe that their observation reflected true thin-film Nb behavior, but was the result of elevated hydrogen concentration at the above-mentioned voids.[13] Furthermore, it could be argued that bulklike behavior should be more representative of films at equilibrium with respect to cycling-induced plastic deformation. But the opposite seems to be true. The question naturally arises if these disparate observations fall under a unifying rule of behavior. The present work attempts to answer this question.

A series of XRD lattice strain measurements versus deuterium (hydrogen) concentration in epitaxial $(1\bar{1}0)$ Nb on *a*-plane sapphire is presented later. Two different films were used, with thicknesses of 208 and 1102 Å. The deuterium concentration was measured *ex situ* using $^2\mathrm{D}(^3\mathrm{He},p)^4\mathrm{He}$ nuclear reaction analysis (NRA). The availability of this technique was in fact the reason for using deuterium instead of hydrogen. Strain in three orthogonal directions, the out-of-plane $[2\bar{2}0]$, the in-plane [110], and the in-plane [002], were measured as the samples were driven through the α-α' miscibility gap below the critical point. This allowed the solid solution and deuteride unit cell parameters to be determined at the miscibility gap boundaries. In addition, the glancing-angle reflectivity response was simultaneously measured and provided the overall film thickness expansion.

II. EXPERIMENTAL DETAILS

The Nb films were grown under MBE conditions on *a*-plane sapphire. Specifically, a substrate temperature of 800 °C, a growth rate of 0.33 ML/s, and a pressure less than 10^{-9} Torr were used to grow two samples with thicknesses of 208 and 1102 Å. These thickness values were determined from the XRD data (see Sec. III). The following orientation relationship exists for the Nb-Al_2O_3 system[14]: $[1\bar{1}0]\|[11\bar{2}0]$; $[111]\|[0001]$; $[11\bar{2}]\|[\bar{1}100]$. The close-packed $(1\bar{1}0)$ bcc plane therefore grows parallel to the $(11\bar{2}0)$ *a*-plane sapphire surface. The substrate miscut angle influences the surface topography of epitaxial Nb films.[15] Miscut angles of order 1 degree lead to a faceted surface morphology that would prevent glancing-angle reflectivity analysis. Miscut angles less than 0.1 deg result in smooth surfaces. The sapphire substrates used here were "epipolished," 0.5 mm thick, and had a miscut angle of 0.05 deg. Both samples were capped with a 30 Å Pd layer to facilitate hydrogen absorption. The Pd cap was grown with the substrate at room temperature to prevent interdiffusion. Atomic force microscopy measurements of the as-deposited films (not shown) indicated a rms surface roughness of approximately 3 Å over a 25 μm^2 area.

The *in situ* XRD measurements were performed at the Advanced Photon Source at Argonne National Laboratory using the UNICAT 33-BM beamline. This beamline is equipped with a Huber four-circle goniometer. The incident x-ray wavelength was either 0.7237 Å for the 1102 Å film or 0.7510 Å for the 208 Å film. An environmental gas cell with a welded circumferential Be window was used for the *in situ* measurements. This cell had gas handling/vacuum ports and two electric feedthrough ports for resistive sample heating, thermocouple temperature measurement, and four-point resistivity measurement. *In situ* resistivity was used to correlate the *ex situ* NRA-based deuterium concentration measurements to the phase transformation, as described below. The out-of-plane strain was measured in symmetric reflection geometry using the $(2\bar{2}0)$ reflection. The in-plane strains were measured in symmetric transmission geometry using the (110) and (002) reflections. Strains were determined from the 2θ peak location in the θ-2θ radial scans. Unit cell parameters of both the solid solution and deuteride phases were determined from a least-squares fit of the four angular coordinates (corresponding to the four rotation axes of the four-circle goniometer) of the three orthogonal reflections.

The *in situ* XRD measurements of both films were performed at slightly elevated temperatures to facilitate the

phase transformation kinetics; the 1102 Å film was held at 80 °C and the 208 Å film was held at 50 °C. The overriding goal of this work was the characterization of lattice strain within the miscibility gap. Both temperatures were chosen to ensure that the films remained below the critical point, a condition confirmed by the discontinuous phase transformation observed in the XRD measurements. Both films were exposed to a saturating deuterium gas pressure (~50 Torr) at the start of the *in situ* experiments. This was done because beam time constraints and very slow *in situ* kinetics prevented true isothermal measurements. In fact, the complete *in situ* $\alpha \rightarrow \alpha'$ phase transformation required 10 to 20 h. The slow kinetic response was attributed to relatively poor vacuum conditions ($\sim 10^{-4}$ Torr) for the *in situ* experimental configuration. The kinetics improved dramatically (of order 0.1 h) under 10^{-7} Torr vacuum conditions. It follows that the surface-mediated absorption of deuterium into the film, not the phase transformation, was the rate limiting step during the *in situ* experiments. The samples were therefore in a state of quasiequilibrium with respect to the ongoing phase transformation.

Pre- and post-exposure characterization of both samples was performed using a Philips X'pert diffractometer at the UIUC Frederick Seitz Materials Research Laboratory (FS-MRL). This instrument has a Cu Kα source ($\lambda = 1.540\,56$ Å), a four-bounce Ge monochromator, and a three-bounce Ge analyzer for high resolution analysis (0.0014 deg Gaussian standard deviation). Characterization measurements with this instrument were performed at room temperature in air in symmetric and asymmetric reflection geometry.

NRA was performed at the UIUC FS-MRL by placing the as-loaded samples in a 0.7 MeV ^{3}He ion beam and recording ion emission spectra in backscatter geometry. These spectra consisted of peaks from backscattered ^{3}He ions from Nb and the two reaction products. (The substrate backscatter ledge was below the energy cutoff of the lower-level discriminator.) The proton energy (13 MeV) from this reaction was too large for complete energy deposition, but this is inconsequential, while the ^{4}He ions (~2 MeV) were completely stopped within the 150 μm depletion layer of the Si surface barrier detector. The incident ^{3}He energy corresponded to the peak of the differential cross section and therefore maximized the reaction rate in the Nb surface layer. The deuterium atomic fraction N_D/N_{Nb} is given by

$$\frac{N_D}{N_{Nb}} = \frac{d\sigma_{RBS} Y_{NRA}}{d\sigma_{NRA} Y_{RBS}}, \tag{1}$$

where the differential angular cross sections $d\sigma_{RBS}$ and $d\sigma_{NRA}$ are evaluated in the laboratory reference frame for backscattered ^{3}He and either reaction product, respectively, and Y_{RBS} and Y_{NRA} are the respective yields.

Ex situ NRA was used to determine the deuterium concentration at the start and end of the miscibility gap for each sample after the XRD measurements. The resistivity profiles of epitaxial Nb films exhibit distinguishable features that delineated the miscibility gap.[16] Both films were loaded with deuterium in the environmental cell at the same temperatures used for XRD analysis, first to the start of gap and then to the end. The resistivity profile was used as a guide. The samples were removed from the environmental cell after each loading step and characterized with NRA. Adequate signal-to-noise ratios were obtained in approximately 30 minu. Deuterium desorption kinetics from epitaxial Nb are nonexistent at room temperature, even under vacuum. This was confirmed during the *in situ* XRD measurements and during the NRA measurements—spectra recorded at 30 minute intervals over the course of several hours did not exhibit significant changes in the reaction-product yields. Thus, the NRA-determined deuterium concentrations are representative of the concentrations that define the miscibility gap at the *in situ* measurement temperature of each film.

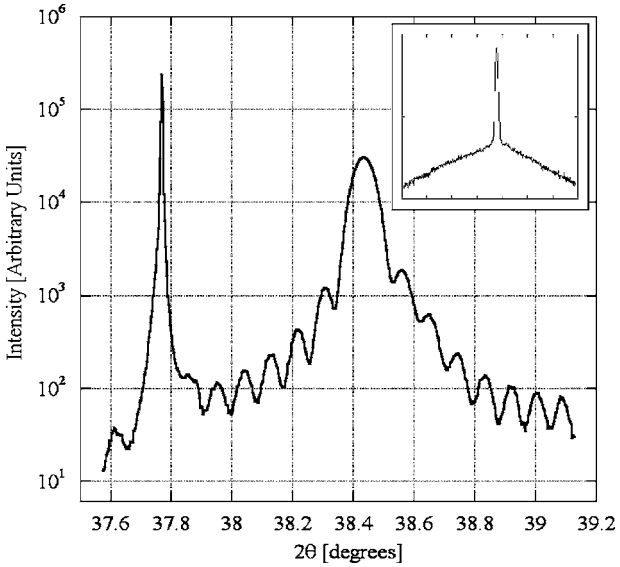

FIG. 1. The first-order specular scan of the pre-exposure 1102 Å film ($\lambda = 1.540\,56$ Å). The sharp peak to the left is the sapphire substrate $(11\bar{2}0)$ reflection and the broad peak to the right is the $(1\bar{1}0)$ Nb reflection. The inset shows the rocking curve scan of the $(1\bar{1}0)$ Nb reflection.

III. EXPERIMENTAL RESULTS

Pre-exposure specular scans (θ-2θ radial scans in symmetric reflection geometry) of the 1102 and 208 Å films are shown in Figs. 1 and 2, respectively. The insets show rocking curves (scans orthogonal to the specular scan direction) of the Nb $(1\bar{1}0)$ reflection. Both the specular and rocking curve scans are characteristic of epitaxial Nb; superlattice fringes in the specular scan and a narrow component in the rocking curve are both demonstrations of epitaxial film quality. The fringes are directly related to the layer thickness[17] and were used to determine the Nb film thickness quoted for each sample. The narrow component of the rocking curve corresponds to that portion of the film commensurate or in perfect registry, with the substrate—in other words, the epitaxial component of the Nb. The width of the narrow component is a convolution of the Darwin width and the resolution of the diffractometer. In the present case, this corresponds to a

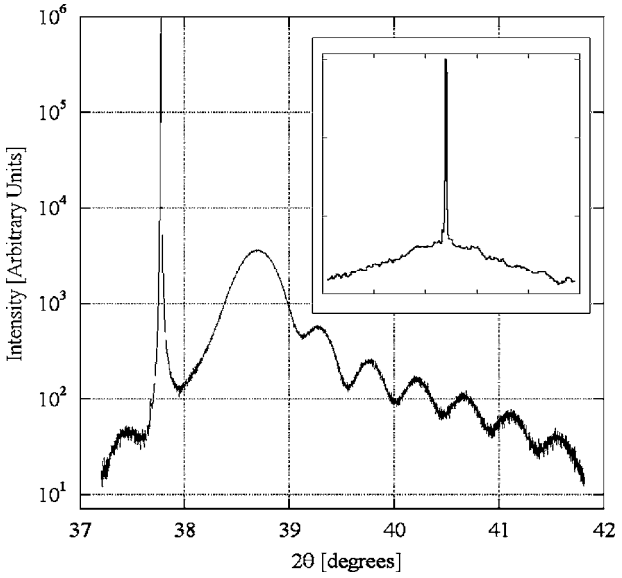

FIG. 2. The first-order specular scan of the pre-exposure 208 Å film ($\lambda = 1.540\,56$ Å). The sharp peak to the left is the sapphire substrate $(11\bar{2}0)$ reflection and the broad peak to the right is the $(1\bar{1}0)$ Nb reflection. The inset shows the rocking curve scan of the $(1\bar{1}0)$ Nb reflection.

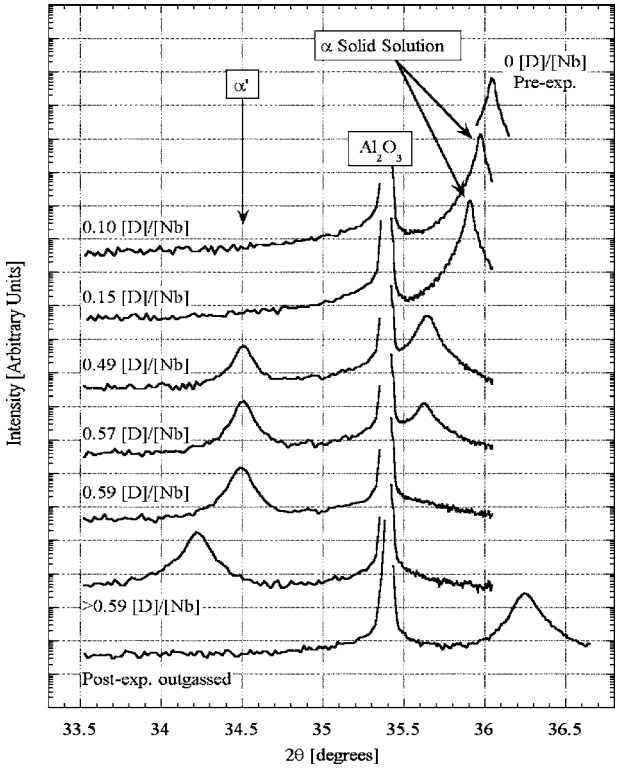

FIG. 3. Second-order specular scans of the 1102 Å film ($\lambda = 0.7237$ Å) during deuterium gas exposure. Deuterium atomic fraction increases from top to bottom, as labeled. The shift of the $(2\bar{2}0)$ Nb reflection due to solid solution deuterium absorption is evident, as is discontinuous $\alpha \rightarrow \alpha'$ phase transformation. The post-exposure, post-outgas scan exhibits compressive strain.

Gaussian standard deviation of approximately 0.002 deg. The broad component of the rocking curve corresponds to material that has lost coherency, as least partially, with respect to the substrate and is no longer commensurate or in perfect registry. The broad component of both samples is on the order of 0.1 deg, a reasonable value for Nb on an *a*-plane sapphire.

The epitaxial Nb volume fraction (out of the total Nb film volume) influences the response of the film during deuteride formation and is given by the ratio of area under the narrow component of the rocking curve to the total area. These ratios are approximately 0.8 and 0.1 for the 208 and 1102 Å films, respectively. The lower epitaxial volume fraction of the thicker film is a consequence of coherency loss during growth. As discussed by Grier *et al.*, a critical thickness exists for perfect epitaxial growth without the formation of dislocations and associated loss of coherency.[14] The in-plane lattice mismatch between $(1\bar{1}0)$ Nb and the $(11\bar{2}0)$ sapphire is very large and coherency loss occurs early in growth. The incommensurate portion of the Nb lattice propagates during growth and results in a lower epitaxial volume fraction for the thicker films. It is the formation of dislocations associated with coherency loss that leads to a nearly strain free Nb lattice, with commensurate regions separated by dislocation-containing incommensurate regions. The dislocation network at the film-substrate interface of the epitaxial Nb-sapphire system has been resolved with transmission electron microscopy by Gutekunst *et al.*[18,19] This work demonstrated that the in-plane lattice mismatch is accommodated by an array of misfit edge dislocations with a spacing of 25 and 140 Å for the case of $(1\bar{1}0)$ Nb on the $(11\bar{2}0)$ sapphire.[19]

The evolution of the second-order specular diffraction intensity during the first deuterium exposure cycle is shown in Figs. 3 and 4 for the 1102 and 208 Å films, respectively. These scans consist of the α and α' $(2\bar{2}0)$ reflections and the second-order reflection from sapphire. The α-α' miscibility gap for the 1102 and 208 Å films is given by atomic ratios of 0.43–0.59 [D]/[Nb] and 0.28–0.45 [D]/[Nb], respectively, as determined by NRA. The peak shift due to the solid solution absorption of deuterium is evident, as is the development of a well-defined α' peak that signals the discontinuous $\alpha \rightarrow \alpha'$ phase transformation in both samples. The specular scan of 1102 Å film after a post-exposure 300 °C vacuum anneal exhibits small compressive strain, while that from the 208 Å film is characterized by a small tensile strain. These two different residual strain states are discussed in the next section.

The dependence of lattice strain on deuterium concentration for both films is shown in Fig. 5. Strain values in the three orthogonal directions were determined from the peak locations on the 2θ scale taken from radial scans. A strain-free bulk Nb lattice constant of 3.3066 Å was used to calculate strain. The location of the sapphire peak provided a check of the calibration of the 2θ scale during deuterium exposure. These data provide the complete picture of the strain state within the film during solid solution deuterium absorption and the ensuing phase transformation. The anisotropic strain in both the solid solution α and deuteride α' phases is revealed as unequal strain values along the three

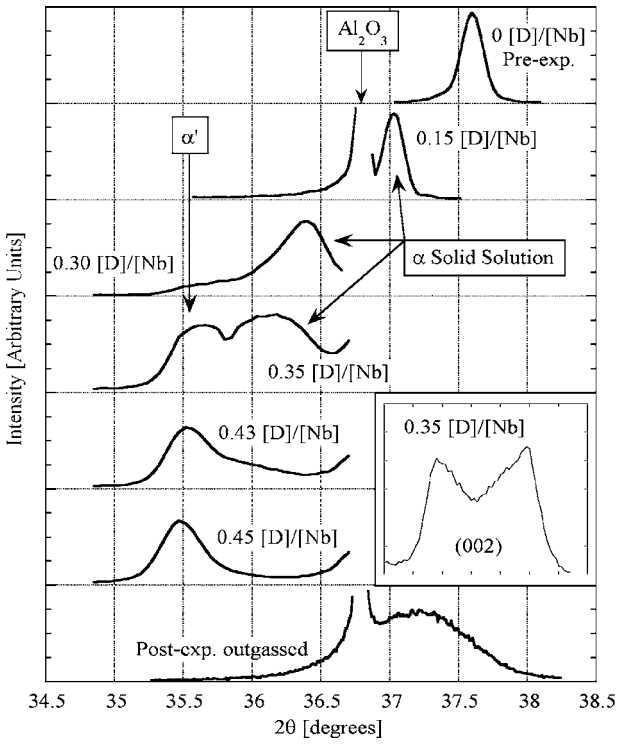

FIG. 4. Second-order specular scans of the 208 Å film ($\lambda = 0.7510$ Å) during deuterium gas exposure. The deuterium atomic fraction increases from top to bottom as labeled. The shift of the $(2\bar{2}0)$ Nb reflection due to solid solution deuterium absorption is evident, as is discontinuous $\alpha \rightarrow \alpha'$ phase transformation. The (002) radial scan (inset) shows the peak splitting associated with the discontinuous transformation more clearly. The post-exposure, post-outgas scan exhibits tensile strain.

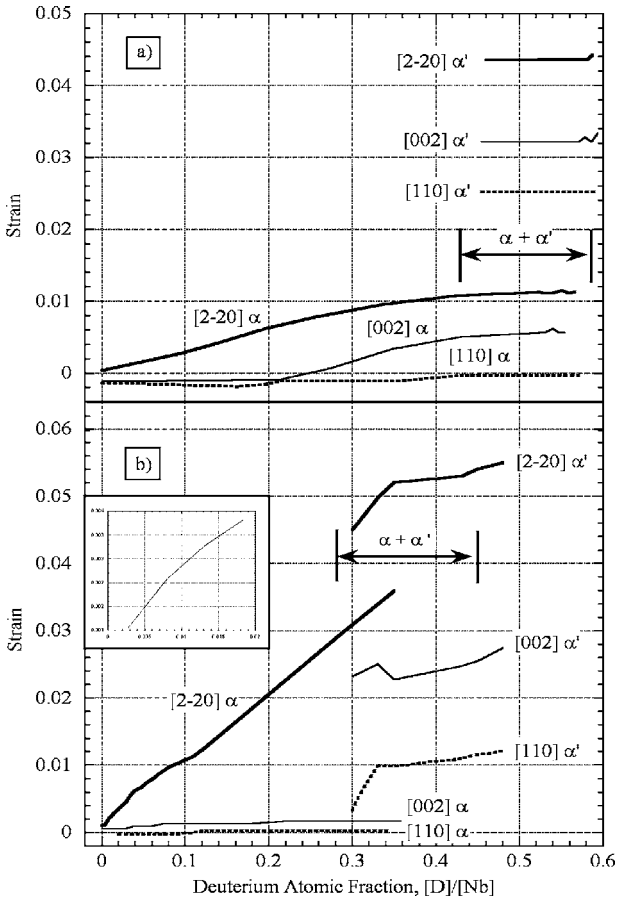

FIG. 5. Dependence lattice strain with deuterium atomic fraction for (a) the 1102 Å film and (b) the 208 Å film. Strains for both the solid solution α phase and the deuteride α' phase in the three orthogonal directions are shown. The $[2\bar{2}0]$ direction corresponds to out of plane, while the [110] and [002] directions are both in plane. The strains are calculated from the 2θ peak positions measured in radial scans. The concentration range of the miscibility gap of each film is identified. The out-of-plane strain observed at a very low concentration in the 208 Å film is shown in the inset.

directions in the lattice. In particular, the out-of-plane strain along the $[2\bar{2}0]$ direction in both phases is enhanced relative to the two in-plane directions. Of greater significance is the different response of the two films within a solid solution; the 208 Å film exhibits the ideal one-dimensional out-of-plane elastic response with very little in-plane slippage, while noticeable strain along the [002] in-plane direction occurred in the 1102 Å film. In fact, the strain along the out-of-plane $[2\bar{2}0]$ direction begins to roll over just as the [002] in-plane strain begins to build. Finally, notice the shift of the miscibility gap to lower deuterium concentration for the 208 Å film. This is simply a demonstration of the reduced overall solubility of deuterium in the thinner film.

The overall film thickness expansion was monitored by simultaneously recording the glancing-angle reflectivity response during deuterium exposure. A comparison of the film thickness expansion and out-of-plane lattice parameter strain is shown in Fig. 6. The film expansion and lattice strain values from the 208 Å film track together reasonably over the entire concentration range. The same is true of the 1102 Å film, but only within the solid solution phase below 0.3 [D]/[Nb]. The two curves for the 1102 Å film begin to diverge as the miscibility gap is approached, with the film thickness expansion becoming a factor of 2 larger than the out-of-plane strain. This behavior is identical to the observations of Rehm *et al.*[13,20] in Nb/Fe multilayers (1000 Å thick Nb component). Enhanced film thickness expansion relative to the lattice strain is therefore a characteristic feature of the 1102 Å film, but not the 208 Å film. As the following discussion illustrates, the enhanced film expansion, or lack thereof, is related to a difference in compliancy of the two films.

IV. ANALYSIS AND DISCUSSION OF RESULTS

The starting point for the analysis of the strain behavior observed here is the strain per unit atomic fraction, otherwise known as Vegard's law, evaluated for bulk Nb,[21]

$$\left.\frac{\Delta a}{a}\frac{1}{C}\right|_{\text{bulk}} = \frac{1}{3}\frac{\Delta \nu}{\Omega} = \frac{1}{3}0.174 = 0.058, \tag{2}$$

where $\Delta\nu/\Omega$ is the atomic volume ratio for deuterium (hydrogen) in bulk Nb and C is the deuterium (hydrogen)

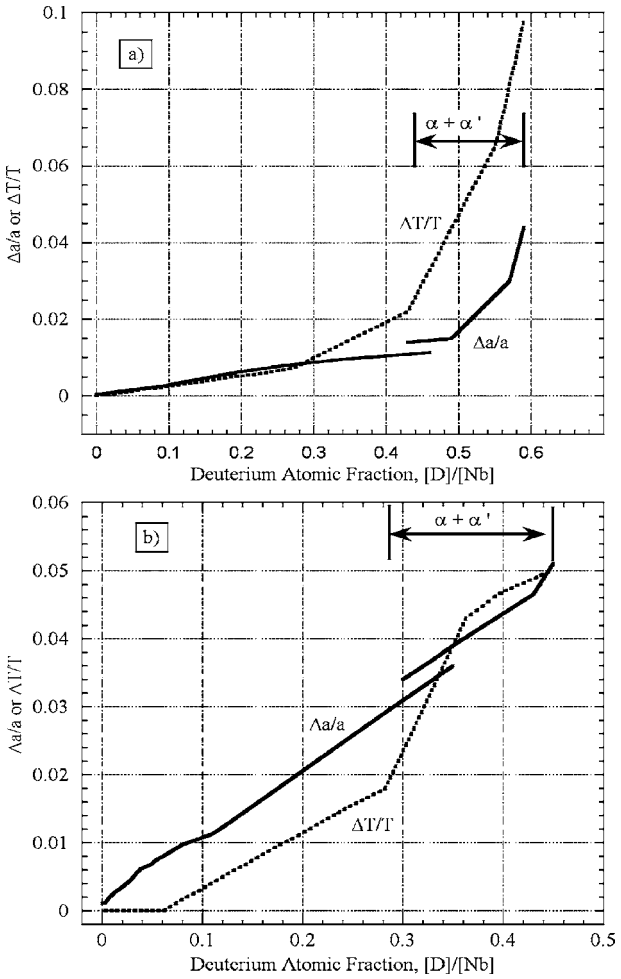

FIG. 6. A comparison of the out-of-plane lattice strain (solid line, $\Delta a/a$) and overall film expansion (dotted line, $\Delta T/T$) versus deuterium atomic fraction for (a) the 1102 Å film and (b) the 208 Å film. Two $\Delta a/a$ curves are shown for each sample, corresponding to the strain in solid solution and the two-phase region. The latter was calculated using a linear combination of strain values for the α and α' phases, weighted by the peak intensity in the radial scans. The divergence of $\Delta T/T$ from $\Delta a/a$ within the miscibility gap of the 1102 Å film is due to dislocation formation associated with the incoherent phase transformation.

atomic fraction in [D]/[Nb] units. This is the expected isotropic response in any Nb lattice direction during deuterium or hydrogen absorption—in other words, the bulk Nb isotropic response.

The anisotropic one-dimensional response expected from a clamped elastic medium along the cubic ⟨110⟩ direction has been derived by Reimer *et al.*,[6]

$$\left.\frac{\Delta a}{a}\frac{1}{C}\right|_{\text{1-D}} = \left.\frac{\Delta a}{a}\frac{1}{C}\right|_{\text{bulk}}\left(1+\frac{C_{11}+3C_{12}-2C_{44}}{C_{11}+C_{12}+2C_{44}}\right)=0.14, \tag{3}$$

where the bulk Nb elastic constants C_{ij} from Ref. 22 were used to evaluate the response. This value represents the enhanced lattice strain expected along the $[2\bar{2}0]$ direction normal to the epitaxial Nb film surface.

TABLE I. A comparison of lattice strain and film expansion responses.

Response	$\Delta a/a$ 1/C	$\Delta T/T$ 1/C	$\Delta V/V$ 1/C
bulk isotropic	0.058	0.058	0.174
1-D	0.14	0.14	0.14
208 Å[a]	0.14	-----	-----
208 Å[b]	0.11	0.07	0.08
208 Å[c]	0.11	0.11	0.22
1102 Å[b]	0.03	0.05	0.05
1102 Å[c]	~0.06	~0.15	0.21

[a]Evaluated over an atomic fraction range of $0 \leqslant [D]/[Nb] \leqslant 0.02$.
[b]Calculated from the origin to the beginning of the $\alpha-\alpha'$ miscibility gap.
[c]Calculated from the origin to the end of the $\alpha-\alpha'$ miscibility gap.

A. Lattice strain

The two behaviors predicted above are compared to the strain versus atomic fraction slopes, as determined from Figs. 5 and 6 data, in Table I. Significant nonlinearity exists within the miscibility gap of the 1102 Å film for both the out-of-plane lattice strain and film thickness expansion behaviors. Two responses are therefore listed in Table I: one from the origin to the beginning of the miscibility gap, the other from the origin to the end of the two-phase region. The same is done for the 208 Å film for consistency, although the differences are much smaller since both $\Delta a/a$ and $\Delta T/T$ track together and are approximately linear.

The first point of discussion concerns the comparison of the observed out-of-plane lattice strain to the predicted behavior. Very good agreement exists between out-of-plane lattice strain and the expected one-dimensional (1-D) response for the 208 Å film. This film did indeed act as an ideal clamped elastic medium. The value of $\Delta\nu/\Omega$ used in Eq. (2) is an average of low-concentration data ($\leqslant 0.03$[D]/[Nb]).[21] A value of $\Delta\nu/\Omega=0.14$ may be more appropriate at higher concentrations within the two-phase region, although not necessarily for bulk single crystal Nb.[21] The predicted bulk and 1-D responses with this value are reevaluated as 0.047 and 0.11, respectively. The inset in Fig. 5(b) indicates a slightly higher slope near the origin. A separate response of the 208 Å film was therefore determined below 0.02 [D]/[Nb] and included in Table I. The agreement between the two observed behaviors and the predicted response at low and high concentration is very good.

The out-of-plane lattice strain observed in the 1102 Å film follows the isotropic response predicted for bulk Nb, although the exact slope depends on the concentration range of the calculation. It is important to note the response of this film initially occurs in the absence of in-plane strain (below 0.3 [D]/[Nb] in Fig. 5(a)); in other words, an approximate bulklike behavior is observed in only one direction, the out-

TABLE II. Pre- and post-cycle strain states.

	208 Å (T=50 °C)		1102 Å (T=80 °C)	
Strain direction	Initial ($\times 10^{-2}$)	Post-cycle ($\times 10^{-2}$)	Initial ($\times 10^{-2}$)	Post-cycle ($\times 10^{-2}$)
$[2\bar{2}0]$	0.11	0.50	0.04	−0.53
[110]	0.06	-----[a]	−0.17	0.73
[002]	−0.02	−0.27	−0.13	0.30

[a]Not measured.

of-plane lattice direction. The response of this film may therefore be identified as pseudoisotropic.

B. Overall film expansion

The overall film thickness expansion, given by $\Delta T/(TC)$ in Table I, is the second point of discussion. The film expansion of the 208 Å film follows the predicted 1-D response, agreeing better with the high concentration 0.11 value rather than the low concentration of 0.14 value. A value for $\Delta T/(TC)$ below 0.02 [D]/[Nb] is not listed in Table I because it was not possible to resolve a change in the film thickness during the early stages of deuterium absorption. The film thickness expansion behavior observed for the 1102 Å film is clearly different from the 208 Å film. The response tracks with the out-of-plane lattice strain in the solid-solution phase up to ~0.3[D]/[Nb], but then diverges from the lattice strain curve. This point of divergence coincides with the development of in-plane strain along the [002] direction. Notice two values of the slope for this film determined from the origin to the end of the gap, $\Delta a/(aC) \sim 0.06$ and $\Delta T/(TC) \sim 0.15$, coincide with the bulk isotropic and clamped 1-D predicted behaviors, respectively. We attribute an enhanced film expansion of the 1102 Å film to dislocation formation associated with the incoherent deuteride phase transformation. We suspect the slippage observed along the [002] direction is a precursory response to the plastic instability associated with deuteride formation.

The re-organization of host Nb atoms during dislocation formation can (and evidently does) lead to enhanced film expansion beyond the observed lattice strain. However, an important caveat is tied to this statement; the residual strain state after deuterium removal should exhibit the effect of this process. Given that the mass transport associated with dislocation formation acts to disproportionately increase the film thickness and that dislocation formation is largely irreversible, we would expect a compressive strain in the $[2\bar{2}0]$ direction after deuterium removal. This is in fact the case, based on the data in Table II, where the initial and post-cycle strain values calculated from the 2θ peak positions are listed. The 1102 Å film experienced a reversal of the out-of-plane strain upon cycling, from slightly tensile to compressive. This reversal is identical to that observed by Yang *et al.*[12] While these authors could not conclusively identify the origin of the strain reversal, we can—the irreversible formation

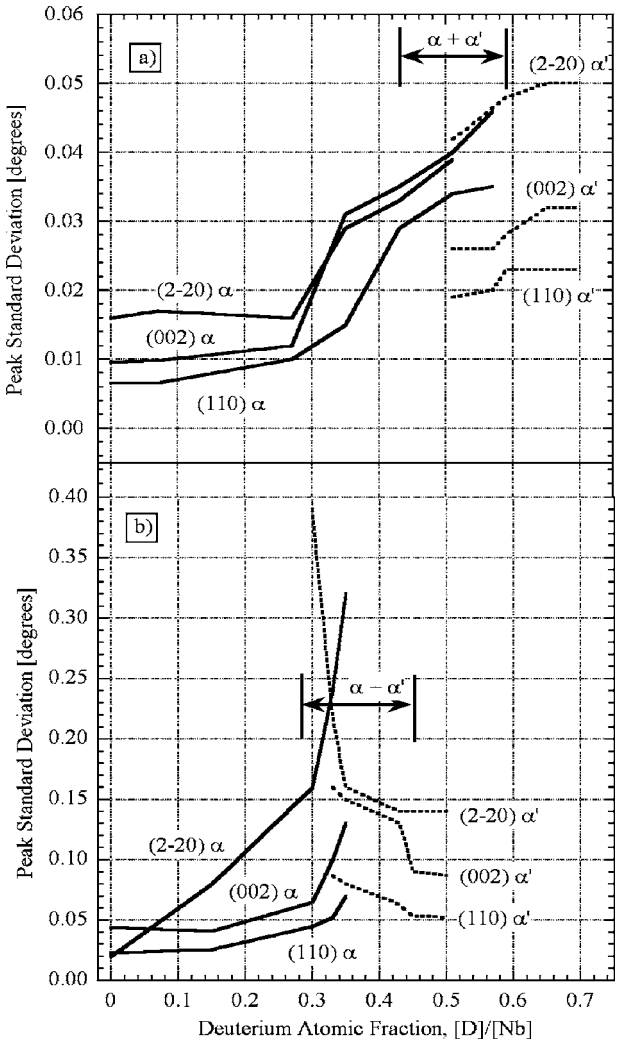

FIG. 7. Gaussian standard deviation versus deuterium atomic fraction for (a) the 1102 Å film and (b) the 208 Å film. The reversible nature of the 208 Å film is consistent with a lack of mosaic broadening from plastic deformation.

of dislocations. The lack of residual compressive strain along the $[2\bar{2}0]$ direction after cycling of the 208 Å film—in fact, a larger residual tensile strain develops after deuterium removal—indicates plastic deformation and associated atomic transport is not as influential in the thinner film.

The strain responses observed here demonstrate a reduced compliancy with respect to plastic deformation for the 208 Å film compared to the 1102 Å film. This statement is supported by (1) the ideal 1-D elastic response; (2) the tracking of out-of-plane lattice strain with overall film thickness expansion, and (3) the lack of residual compressive strain. The more limited deuterium solubility in the 208 Å film, as manifested by the observed shift of the miscibility gap to lower deuterium atomic fractions, is another consequence of this reduced compliancy.

Further evidence of suppressed plastic deformation in the thinner film is given in Fig. 7, a plot of radial peak widths versus deuterium concentration. The peak widths increase as both films approach and enter the miscibility gap. However, this increase is reversible in the thinner film. Reversible be-

TABLE III. Epitaxial Nb unit cell parameters and associated strain determined from XRD analysis.

Parameter	208 Å[a]					1102 Å[a]				
	Pre-exp.	α_{ss}[b]	$\varepsilon(\times 10^{-2})$	α'[c]	$\varepsilon(\times 10^{-2})$	Pre-exp	α_{ss}[b]	$\varepsilon(\times 10^{-2})$	α'[c]	$\varepsilon(\times 10^{-2})$
$a_{[100]}$(Å)	3.238	3.272	1.05	3.344	3.27	3.263	3.284	0.64	3.393	3.98
$a_{[010]}$(Å)	3.390	3.430	1.18	3.510	3.54	3.348	3.368	0.60	3.480	3.94
$a_{[001]}$(Å)	3.315	3.318	0.09	3.408	2.81	3.303	3.326	0.69	3.439	4.12
α(deg)	93.05	93.03		93.25		90.93	90.92		90.93	
β(deg)	88.14	88.15		87.93		88.74	88.74		88.74	
γ(deg)	90.17	91.36		92.53		90.14	90.69		91.51	

[a]Strain values are relative to the pre-exposure unit cell parameters.
[b]Calculated at the beginning of the α-α' miscibility gap.
[c]Calculated at the end of the α-α' miscibility gap.

havior can only occur in the absence of significant mosaic broadening and is the result of strain broadening, particle size broadening, or both. One possible source of strain broadening is coherency strain that develops as the two phases coexist and then dissipates with internal phase boundaries. Reversible particle size broadening could occur as a result of the partitioning of Nb film volume between the two phases, an effect that would also vanish with internal phase boundaries. The peak widths do not recover in the thicker film and therefore signal significant mosaic broadening resulting from plastic deformation. Although the peak width changes reversibly in the 208 Å film as the miscibility gap is crossed once, note that an irreversible increase occurs after one complete cycle. This is evident in Fig. 4, where the post-cycle peak standard deviation is approximately 0.2 degrs.

The less compliant response of the 208 Å film is due to the higher epitaxial volume fraction. A greater portion of the 208 Å film is commensurate with the substrate and therefore able to resist deuteride-induced plastic deformation, at least during the first exposure cycle. In contrast, the bulklike response of the 1102 Å film is the result of the large incommensurate portion of the epitaxial Nb. The larger incommensurate volume accommodates in-plane distortion in a strain-free manner, at least below 0.3 [D]/[Nb], and reduces the observed out-of-plane strain. This accommodation is probably the result of relaxation followed by plasticity within the incommensurate volume, which irreversibly broadens the mosaic. This process of accommodation must be closely coupled to the lattice instability associated with the miscibility gap since the peak widths begin to broaden near 0.3 [D]/[Nb], at just the point where in-plane strain begins along the [002] direction.

C. Volumetric expansion

The third point of discussion is the volumetric expansion data listed in Table I. The volumetric expansion of each film was determined at the beginning and end of the miscibility gap using the unit cell parameters given in Table III. This calculation assumed a completely general triclinic symmetry. The volumetric expansion values for each film within a solid solution are similar and considerably lower than the higher concentration values, which are likewise nearly equal. While the volumetric expansion within the solid solution phase of each film is considerably lower than either predicted volumetric expansion value, the high concentration values are bulklike. This shift from a low $\Delta V/(VC)$ value to a bulklike $\Delta V/(VC)$ value is brought on by the large strains associated with the phase transformation.

These last two statements may appear to contradict the observed strain anisotropy within a two-phase region; in other words, that highly anisotropic strains in three orthogonal directions can lead to an approximate isotropic response of the unit cell. Consideration of the strain data in Table III reveals that the unit cell distortions are reasonably isotropic, especially in the case of the 1102 Å film. The initial angular distortions for both films are significant, approaching and exceeding 3 deg. for the 208 Å film. However, the changes in the angle parameters during deuterium absorption are relatively small, except for γ, the angle between the [100] and [010] directions. In fact, the systematic increase of γ with deuterium absorption is the only significant change in the angle parameters of both films.

It is this change in γ, coupled with the lattice parameter strains, that leads to the observed strain anisotropy in the $[2\bar{2}0]$, [110], and [002] directions. This is apparent from a calculation of the strains along these directions using the unit cell parameters and the law of cosines. The strains calculated this way are compared to the strains determined from the radial 2θ positions in Table IV. Good agreement is found.

D. Comparison of behaviors observed here to the work of others

The following two statements can be made based on the observations presented here:

(1) Thin epitaxial $(1\bar{1}0)$ Nb films respond as ideal clamped elastic media in terms of both the out-of-plane lattice strain and overall film expansion. This response occurs in the complete absence of in-plane strain in the solid solution phase.

(2) Thick epitaxial $(1\bar{1}0)$ Nb films do not respond as ideal clamped elastic media. Instead the response depends on the concentration range and type of behavior (lattice strain or

TABLE IV. A comparison of calculated and measured lattice strain values.

Strain direction	208 Å				1102 Å[a]			
	Calc. α[a] $\varepsilon(\times 10^{-2})$	$2\theta\ \alpha$ $\varepsilon(\times 10^{-2})$	Calc. α'[b] $\varepsilon(\times 10^{-2})$	$2\theta\ \alpha'$ $\varepsilon(\times 10^{-2})$	Calc. α[a] $\varepsilon(\times 10^{-2})$	$2\theta\ \alpha$ $\varepsilon(\times 10^{-2})$	Calc. α'[b] $\varepsilon(\times 10^{-2})$	$2\theta\ \alpha'$ $\varepsilon(\times 10^{-2})$
$[2\bar{2}0]$	2.2	2.9	5.5	5.4	1.1	1.1	5.2	4.4
[110]	0.1	~0	1.3	1.2	0.1	~0	2.7	2.5
[002]	0.1	0.2	2.8	2.6	0.7	0.5	4.1	3.2

[a]Strain values calculated at the beginning of the α-α' miscibility gap from unit cell parameters in Table III.
[b]Strain values calculated at the end of of α-α' miscibility gap from unit cell parameters in Table III.

film expansion). In the solid solution phase, both the out-of-plane lattice strain and film expansion are approximately bulklike, the former occurring without equivalent levels of in-plane strain. In the deuteride phase, the lattice strain remains approximately bulklike, while the film expansion follows the clamped 1-D film behavior.

These two statements comprise a set of rules that can be used to understand the responses of $(1\bar{1}0)$ Nb films observed by others. This discussion is facilitated by Table V, a tabulation of the pertinent results from this work and those of others presented in the Introduction. First, the thin-film entries in the top portion of Table V comprise a consistent set of results exhibiting the expected 1-D response from a clamped elastic medium. This holds for the entire 0-1 [H]/[Nb] concentration range. Textured $(1\bar{1}0)$ Nb is seen to reach this response with cycling. A similar trend with cycling has been observed in a thin textured Pd film.[23]

Inconsistencies are evident for the thick-film data entered in the middle portion of Table V. This is the consequence of statement (2); the observed response from thick Nb films depends on hydrogen concentration and the type of behavior. The lattice strain response for the first three high-concentration results are consistent, while identical film expansion behavior is found for our work and that of Rehm *et al.*[13] at high concentration. The two lower concentration lattice strain results (italicized in Table V) do not agree with the higher concentration results. Our solid solution lattice strain result is too low, but not necessarily in stark disagreement. Furthermore, our film expansion result in solid solution actually does exhibit a bulklike response, as might be expected in the absence of significant plastic deformation associated with deuteride formation. The epitaxial Nb result of Laudahn *et al.*[11] is inconsistent with the rest of the thick-film data, a consequence of the very low concentration used and the lack of plastic deformation. In fact, the out-of-plane lattice strain observed by Laudahn *et al.* begins to roll over at higher hydrogen concentration toward a lower $\Delta a/(aC)$ value, but this trend was not followed to high concentration.

The thick textured film result of Laudahn *et al.* (the third block of data in Table V) exhibits a 1-D response at low concentration and therefore is not consistent with the other

TABLE V. A comparison of out-of-plane lattice strain and film thickness expansion of epitaxial and textured $(1\bar{1}0)$ Nb.

Reference	Microstructure[a]	Thickness (Å)	[H]/[Nb] Range	$\Delta a/a\ 1/C$	$\Delta T/T\ 1/C$
10	Epi. SL	320	0–0.8	0.1	
12	Text. ML	140	0–0.3	0.05[b]–0.13[c]	
This work	Epi. SL	208	0–0.02	0.14	
This work	Epi. SL	208	0–0.28	0.11	0.07
This work	Epi. SL	208	0–0.45	0.11	0.11
10	Epi. SL	720	0–1	0.06	
13	Text. ML	1000	0–1	0.06	0.14
This work	Epi. SL	1102	0–0.59	0.06	0.15
This work	*Epi. SL*	*1102*	*0–0.43*	*0.03*	*0.05*
11	*Epi. SL*	*1900*	*0–0.04*	*0.13*	
11	Text. SL	1900	0–0.08	0.13	
11	Text. SL	1900	0–0.2	0.11	
6	*Epi. SL*	*2500*	*0–0.02*	*0.5*	

[a]Epi.—epitaxial Nb from MBE; Text—textured Nb from sputtering deposition, laser deposition, or electron beam evaporation; SL—single layer film; ML—multilayer film.
[b]First cycle.
[c]Third cycle.

thick-film results (except for their own thick epitaxial result). Like the epitaxial data of Laudahn *et al.*, these data begin to roll over at higher concentration, as reflected in the reduced slope when the calculation is extended to 0.2 [H]/[Nb]. Two possible explanations for this inconsistency exist: (1) the 1-D behavior is the true response of thick textured Nb films, or (2) the higher slope is the result of the limited concentration range. The argument in support of (1) is that textured films already contain dislocations involved in the tilt boundaries associated with the large mosaic structure. The accommodation that occurs in thick epitaxial Nb films and limits the observed strain may therefore not play a significant role, perhaps because the film is prehardened with respect to deformation. This could lead to the 1-D response. We note that the same 1-D response for *film expansion* has been observed at high deuterium concentrations in thick textured Pd films.[23] The argument in support of (2) is the lower slope trend at a higher concentration inherent in the Laudahn *et al.* data.

Finally, the last result in Table V is in such severe contrast to all other results that it must be discounted. Reimer *et al.*[6] employed the $^{15}N(p,\alpha\gamma)^{12}C$ resonance reaction to measure the absolute hydrogen concentration. These authors assumed the native Nb oxide prevented hydrogen evolution at room temperature during the two-step (XRD followed by the resonance reaction measurements) experimental investigation. The hydrogen concentration range investigated by Reimer *et al.* was very low, and we suspect a systematic error in the concentration determination. Absolute hydrogen concentration measurement using this technique requires a hydrogen-containing calibration standard or absolute determination of ion beam current, γ-detector solid angle, and γ-detector efficiency (relative depth profile measurements are free from these sources of systematic error). Unfortunately, specific experimental details regarding the use of the resonance reaction technique were not provided by Reimer *et al.* Alternatively, hydrogen evolution from the Nb between the XRD and resonance reaction measurements could explain the anomalous lattice expansion result.

V. CONCLUSIONS

Based on the measurements presented here, the out-of-plane lattice strain and film expansion behavior of epitaxial Nb is governed by a single rule; epitaxial Nb responds either as an ideal clamped 1-D elastic medium or as a pseudoisotropic bulk medium, depending on the film thickness. This rule unifies the past work of others, with a few noted exceptions, to the measurements presented here. The point of differentiation between these two responses is a film thickness between the two used here, 208 and 1102 Å, and is determined by the volume fraction of Nb commensurate with the single crystal substrate. The amount of commensurate material determines whether the film acts compliantly or noncompliantly with respect to plastic deformation associated with deuteride (hydride) formation.

Thick films with a low commensurate volume fraction are compliant and therefore exhibit a bulklike response. In this case, relaxation and/or plasticity facilitated by the large incommensurate film volume leads to reduced out-of-plane strain and reduced in-plane strain early in the solid solution. The plasticity associated with this process causes eventual in-plane slippage, irreversible mosaic broadening, larger deuterium solubility, enhanced film thickness expansion, and a compressive residual strain after cycling. The film thickness expansion follows the 1-D behavior of a clamped medium, but this is considered fortuitous since there is no prevailing reason why this should be the case. The nonlinear out-of-plane lattice strain and film thickness expansion observed in the two-phase region lends support to this statement.

Thin films are much less compliant because of the greater commensurate volume fraction and this leads to a true 1-D elastic response without any in-plane strain. The evidence of reduced plasticity includes lower deuterium solubility, reversible peak broadening, lack of enhanced film thickness expansion, and a residual tensile strain state.

Noticeable strain anisotropy was observed in the three orthogonal lattice directions probed with XRD at the beginning and end of the two-phase region of both films. This anisotropy is a consequence of isotropic strain distortions of the Nb unit cell coupled to a systematic increase of the angle γ between the [100] and [010] directions.

ACKNOWLEDGMENTS

This work was supported by the U.S. National Science Foundation under Grant No. DMR-9982520. The UNICAT facility at the APS is supported by the U.S. DOE under Award No. DEFG02-91ER45439, through the UIUC FS-MRL, the Oak Ridge National Laboratory (U.S. DOE Contract No. DE-AC05-00OR22725 with UT-Battelle LLC), the National Institute of Standards and Technology (U.S. Department of Commerce) and UOP LLC. The APS is supported by the U.S. DOE, Basic Energy Sciences, Office of Science under Contract No. W-31-109-ENG-38. The Center for Microanalysis of Materials at the UIUC FS-MRL is partially supported by the U.S. Department of Energy under Award No. DEFG02-91-ER45439. The use of the UNICAT, APS, and CMM facilities are gratefully acknowledged.

The authors are grateful to Dr. I. Petrov (UIUC) for supplying the He-3 gas for the NRA measurements, Dr. C. Durfee (UIUC, now with Intel) for the growth of the epitaxial Nb films, Dr. P. Zschack and Dr. E. Karapetrova (UIUC UNICAT) for assistance with beamline use at the APS, Dr. M. Sardela (UIUC) for help with XRD analysis using the Philips equipment, Dr. R. Averback (UIUC) for help with NRA data interpretation, S. Sprague (UIUC) for fabrication of the environmental measurement cell, M. Williams (UIUC) for assistance with the NRA measurements, and H. Ju (UIUC) for XRD analysis of selected samples. Finally, Dr. P. Ransom (UIUC) and the UIUC SURGE program are gratefully acknowledged.

*Current address: Exelon Nuclear, Warrenville, Illinois 60555, USA.
†Email: bheuser@uiuc.edu

[1] P. F. Miceli and H. Zabel, Phys. Rev. Lett. **59**, 1224 (1987).
[2] P. F. Miceli and H. Zabel, Z. Phys. B: Condens. Matter **74**, 457 (1989).
[3] P. F. Miceli, H. Zabel, J. A. Dura, and C. P. Flynn, J. Mater. Res. **6**, 964 (1991).
[4] A. Gibaud, R. A. Cowley, D. F. McMorrow, R. C. C. Ward, and M. R. Wells, Phys. Rev. B **48**, 14463 (1993).
[5] G. Alefeld, Ber. Bunsenges. Phys. Chem. **76**, 746 (1972).
[6] P. M. Reimer, H. Zabel, C. P. Flynn, A. Matheny, K. Ritley, J. Steiger, S. Blässer, and A. Weidinger, Z. Phys. Chem. **181**, 367 (1993).
[7] G. Song, M. Geitz, A. Abromeit, and H. Zabel, Phys. Rev. B **54**, 14093 (1996).
[8] G. Song, A. Remhof, K. Theis-Bröhl, and H. Zabel, Phys. Rev. Lett. **79**, 5062 (1997).
[9] E. Johansson, S. Olsson, C. Chacon, and B. Hjörvarsson, J. Phys.: Condens. Matter **16**, 1165 (2004).
[10] A. Abromeit, R. Siebrecht, G. Song, H. Zabel, F. Klose, D. Nagengast, and A. Weidinger, J. Alloys Compd. **253–254**, 58 (1997).
[11] U. Laudahn, A. Pundt, M. Bicker, U. v. Hülsen, U. Geyer, T. Wagner, and R. Kirchheim, J. Alloys Compd. **293–295**, 490 (1999).
[12] Q. M. Yang, G. Schmitz, S. Fähler, H. U. Krebs, and R. Kirchheim, Phys. Rev. B **54**, 9131 (1996).
[13] Ch. Rehm, H. Fritzsche, H. Maletta, and F. Klose, Phys. Rev. B **59**, 3142 (1999).
[14] E. J. Grier, M. L. Jenkins, A. K. Petford-Long, R. C. C. Ward, and M. R. Wells, Thin Solid Films **358**, 94 (2000).
[15] G. L. Zhou and C. P. Flynn, Phys. Rev. B **59**, 7860 (1999).
[16] B. J. Heuser, H. Onumah and M. C. Allain, J. Alloys Compd. (to be published).
[17] B. E. Warren, *X-Ray Diffraction* (Dover, New York, 1990).
[18] G. Gutekunst, J. Mayer, and M. Rühle, Philos. Mag. A **75**, 1329 (1997).
[19] G. Gutekunst, J. Mayer, V. Vitek, and M. Rühle, Philos. Mag. A **75**, 1357 (1997).
[20] Ch. Rehm, H. Maletta, M. Fieber-Erdmann, E. Holub-Krappe, and F. Klose, Phys. Rev. B **65**, 113404 (2002).
[21] H. Peisl, *Topics in Applied Physics: Hydrogen in Metals I*, edited by G. Alefeld and J. Völkl (Springer-Verlag, Berlin, 1978), Vol. 28
[22] D. I. Bolef, J. Appl. Phys. **32**, 100 (1961).
[23] A. E. Munter and B. J. Heuser, Phys. Rev. B **58**, 678 (1998).